The 2010 IEEE/RSJ International Conference on
Intelligent Robots and Systems
October 18-22, 2010, Taipei, Taiwan

Gain Scheduled Control of Perturbed Standing Balance

Dengpeng Xing, Christopher G. Atkeson, Jianbo Su, and Benjamin J. Stephens

Abstract— **This paper develops full-state parametric controllers for standing balance of humanoid robots in response to impulsive and constant pushes. We also explore a hypothesis that postural feedback gains in standing balance should change with perturbation size. From an engineering point of view this is known as gain scheduling. We use an optimization approach to see if feedback gains should scale with the perturbation for a simulated robot. We simulate models in the sagittal and lateral plane and in 3-dimensions, use a horizontal push of a given size, direction and location as a perturbation, and optimize parametric controllers for different push sizes, directions and locations. During a simulated perturbation experiment, the appropriate controller is continuously selected based on the current push. For an impulse, the simulated robot recovers back to the initial state; for a constant push, the robot moves to an equilibrium position which leans into the push and has zero joint torques. We show the performance of optimized parametric controllers in response to different external pushes.**

I. Introduction

Balance research adapts humanoid robots to complex human environments and is also valuable to explore how humans react to disturbances. In [1], a passivity-based full-body balancing strategy is proposed to accommodate an arbitrary number of external force interaction points. In [2], an integral balance controller is proposed to allow a humanoid robot to recover from large disturbances. In [3], multiple strategies are used for standing balance arising from the same optimization criterion. By using Differential Dynamic Programming (DDP), a trajectory library representing an optimized control policy is generated for standing balance on an adaptive grid [4].

A trajectory library stores optimized policies for different cases and chooses an appropriate controller for each push. Compared with it, parametric feedback has many advantages: it can produce feedback responses with a small number of parameters, while a trajectory library needs much more storage for each posture and push; a feedback controller has a smaller computational cost, and with optimized parameters can handle complex models and cases. However, one set of parameters might not handle all possible perturbations. This paper explores optimizing postural feedback controllers for external perturbations with a variety of sizes, locations and directions.

Many papers have been presented on human standing balance in terms of feedback controllers responding to disturbances. In [5], optimal control and state estimation are employed to explain selection of control strategies used by humans, in response to small perturbations to stable upright balance. A linearized model and Linear Quadratic Regulators (LQR) are used for optimization. Park *et al.* [6] tests human postural responses in terms of a feedback control system with feedback gains that are gradually scaled with perturbation size and can accommodate biomechanical constraints. In [7], using a 3-link sagittal model, equilibrium maintenance during standing is investigated in humans by using eigenvectors of the motion equation. Data analysis in human standing experiments shows independent feedback control of movements can adequately describe human postural responses to stance perturbations and is sufficient to provide stability [5]-[7].

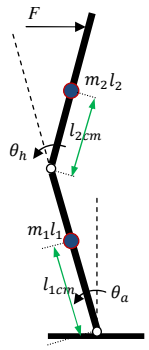

Fig. 1. Two-link inverted pendulum model in the sagittal plane.

Most research focuses on instantaneous perturbations in the sagittal plane and designs various controllers to respond to impulses and move back to the upright state. In reality, disturbances may push in many directions and act for a finite time during which the push size, direction and location may also change. Often policies for impulses can not handle constant pushes, so controllers for both impulsive and constant disturbances are required for standing balance. We design linear feedback controllers for impulsive and constant pushes, respectively, explore standing balance in the sagittal and lateral plane and in 3-dimensions and use an optimization approach to test if the optimized feedback gains should scale with the perturbation size for a simulated robot. The validity and performance of the proposed controllers are explored using simulation.

II. Balance Controller in the Sagittal Plane

This study uses a two-link inverted pendulum model in the sagittal plane, with actuators located at the ankle and hip joints, as shown in Fig. 1. The model is facing to the right,

Dengpeng Xing and Jianbo Su are with the Department of Automation, Shanghai Jiao Tong University, Shanghai, China. xingdengpeng@hotmail.com, jbsu@sjtu.edu.cn
Christopher G. Atkeson and Benjamin J. Stephens are with the Robotics Institute, Carnegie Mellon University, Pittsburgh, PA, USA. cga@cmu.edu, bstephens@cmu.edu

and the parameters are listed in Table I, where l_i, m_i, l_{icm} and MoI_i represent the length, mass, center of mass (CoM) relative to the lower joint and moment of inertia about the CoM of the corresponding link. The robot joint limits are $-0.52 < \theta_a < 0.79$ radians and $-2.18 < \theta_h < 0.52$ radians, where θ_a is the ankle angle, θ_h is the hip angle, and $\theta_i = 0$ is the upright state. The ankle torque is limited within $\pm$50Nm to prevent the foot from tilting, and the maximum of hip torque is $\pm$157Nm. Robot parameters in this paper are taken from a preliminary design of a planned humanoid.

A. Balance Controller

We define the state as ankle and hip angles and angular velocities. The robot sagittal dynamics are:

$$\mathbf{x}(k+1) = \boldsymbol{f}(\mathbf{x}(k), \tau(k), F(k), r(k)), \tag{1}$$

where $\mathbf{x} = (\theta_a, \theta_h, \dot{\theta}_a, \dot{\theta}_h)^{\mathrm{T}}$ is the state vector, $\tau = (\tau_a, \tau_h)^{\mathrm{T}}$ represents the joint torques, and F and r are the push size and location.

We consider a feedback controller which acts on the error in each state variable:

$$\begin{aligned} \tau_a &= -k_1\Delta\theta_a - k_2\Delta\theta_h - k_3\Delta\dot{\theta}_a - k_4\Delta\dot{\theta}_h, \\ \tau_h &= -k_5\Delta\theta_a - k_6\Delta\theta_h - k_7\Delta\dot{\theta}_a - k_8\Delta\dot{\theta}_h, \end{aligned} \tag{2}$$

where

$$\begin{aligned} \Delta\theta_a &= \theta_a - \theta_{a\_d}, \qquad & \Delta\theta_h &= \theta_h - \theta_{h\_d}, \\ \Delta\dot{\theta}_a &= \dot{\theta}_a - \dot{\theta}_{a\_d}, \qquad & \Delta\dot{\theta}_h &= \dot{\theta}_h - \dot{\theta}_{h\_d}, \end{aligned}$$

represent the error between ankle and hip actual state and the desired state for the current push. The torque outputs from the controller are limited as described earlier.

B. Optimization Criterion

We define the one step optimization cost function as a weighted sum of the squared deviations of state error and the joint torque magnitude:

$$\boldsymbol{L}(\mathbf{x}, \mathbf{u}) = \mathrm{T}\Delta\mathbf{x}^{\mathrm{T}}\mathbf{Q}\Delta\mathbf{x} + \mathrm{T}\tau^{\mathrm{T}}\mathbf{R}\tau, \tag{3}$$

where T is the time step of the simulation (0.01s), $\mathbf{Q} = \mathbf{I}_{4\times4}$ and $\mathbf{R} = 0.02 \cdot \mathbf{I}_{2\times2}$ are the weight matrices, where $\mathbf{I}$ is the identity matrix and 0.02 weights the torque penalty relative to the state error in order to decrease the response time of the optimized controller. The total cost is the sum of the one step cost function over time. We use this cost function as an optimization criterion to find the minimum of total cost for each push, optimizing the parameters of the feedback controller.

TABLE I
THE PARAMETERS OF ROBOT LATERAL MODEL.

Link	Length(m)	CoM(m)	Mass(kg)	MoI(kg·m^2)
Calf	0.3305	0.2645	4.8685	0.1741
Thigh	0.3305	0.2645	4.8685	0.1741
Pelvis	0.1778	0.0889	7.373	0.2584
Torso	0.653	0.1407	22.119	0.7752

C. Optimization Approach

The controller parameters are optimized for both impulsive and constant pushes, respectively, using a number of sizes and locations. We assume all pushes are horizontal, as vertical pushes have little effect. An impulsive push exists for a short period of time (0.1 second in this paper), and we choose the upright state as the desired state. For a constant push, based on each push size and location, we first calculate an equilibrium state, which is the posture where the robot leans into the push and the torques at the ankle and hip are zero. We use this equilibrium state as the desired state, rather than standing straight up. Instead of optimizing from one initial state such as standing vertically, we choose a set of initial states which evenly separate the range between the state of standing vertically and the equilibrium state.

SNOPT is a general-purpose system for constrained optimization, using sequential quadratic programming (SQP) [8]. We employ it to optimize controller parameters for each push, using the LQR gain for standing upright as initial values for our controller and optimizing the next push size with the optimized gains of the previous case. For a constant push, with the given size and location, we randomly choose five initial states for each joint including the posture where the robot stands straight. The cost of the trajectory from each initial state is combined, with a penalty added for the cases violating state constraints. Optimized parameters can be generated for a wide range of pushes. The robot looks the desired state and feedback gains based on the push force and location.

D. Results

We use constant pushes to explore postural feedback gains, supposing the push is acting at the head. Fig. 2 shows the optimized gains for constant pushes at the head. The gains are symmetric when the robot is pushed forward and backward, except for the extreme values due to the asymmetric state constraints. With a small push, i.e. less than 30N, K1 ($\Delta\theta_a \rightarrow \tau_a$) is the largest gain with a value above 620Nm/rad. The other three position gains are relatively small, with values no more than 100Nm/rad. K3 ($\Delta\dot{\theta}_a \rightarrow \tau_a$) is the largest velocity gain, 170Nm·s/rad, and the other three velocity gains have less effect, with less than 30Nm·s/rad magnitude. It is also found that, for small push sizes, the gains gradually scale with push magnitude, with K5 ($\Delta\theta_a \rightarrow \tau_h$) and K6 ($\Delta\theta_h \rightarrow \tau_h$) increasing fastest and ankle torque gains related to velocities almost unchanged.

With larger pushes (beyond 30N), each gain changes much more with push magnitude, with the ankle gains increasing and the hip gains becoming more negative. The hip gains comparatively exhibit more change than the ankle gains. The most significant changes are for the gains of hip torque relative to ankle angle and velocity. For ankle gains, $\tau_a/\dot{\theta}_a$ and $\tau_a/\dot{\theta}_h$ change the most. Note that K5, K7, and K8 become negative as the push size increases, with the extreme values on the order of -370Nm/rad, -230Nm·s/rad and -23Nm·s/rad respectively. The negative hip gains and the positive ankle gains take advantage of large hip flexing to

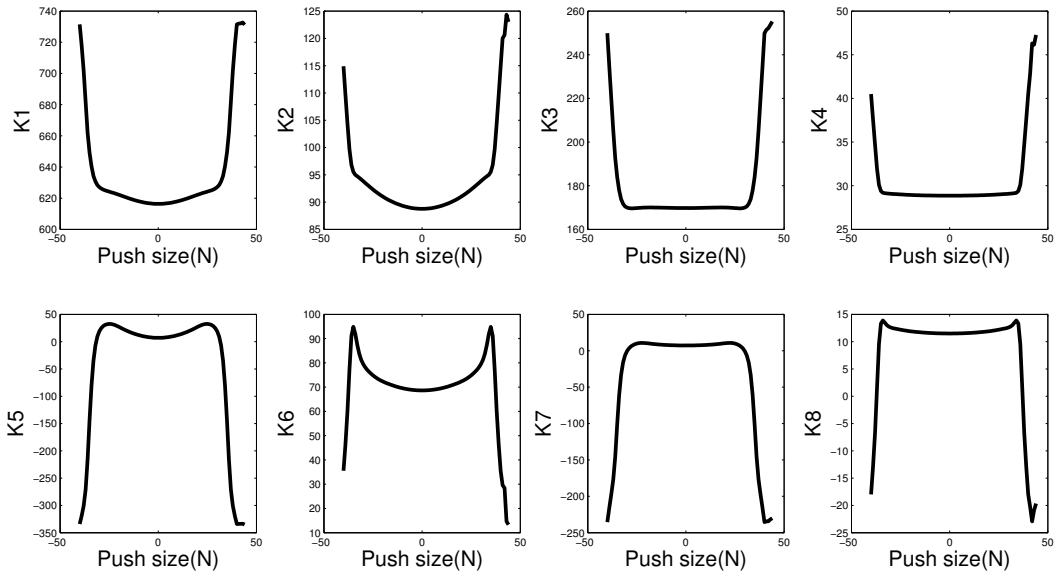

Fig. 2. The gains of the proposed controller for constant pushes at the head.

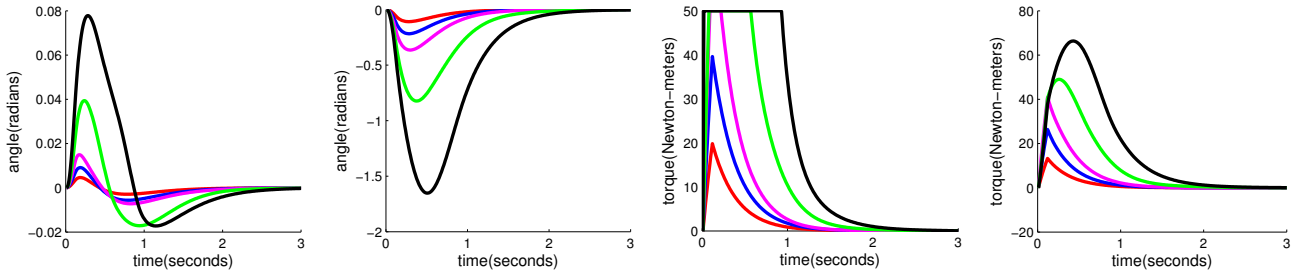

(a) Ankle angle (b) Hip angle (c) Ankle torque (d) Hip torque

Fig. 3. Simulated angle and torque trajectories for a range of impulsive perturbation sizes (2.5, 5, 8, 10, 11 Newton-seconds).

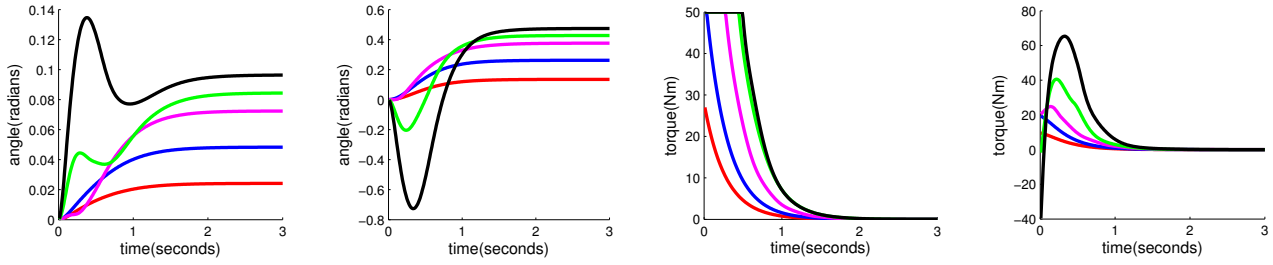

(a) Ankle angle (b) Hip angle (c) Ankle torque (d) Hip torque

Fig. 4. Simulated angle and torque trajectories for a range of constant perturbation sizes at the head (10, 20, 30, 35, 40 Newtons).

initially move the ankle and the hip in the push direction, which helps maintain balance when the robot responds to large perturbations.

Fig. 3 shows the angle trajectories and the corresponding torques of the proposed controller for a range of impulsive push sizes located at the head. Angles and torques roughly scale with push magnitude, except ankle torques saturate for larger perturbations. The hip angle is entirely negative whereas the ankle joint initially grows in the positive direction and changes to negative shortly after the hip reaches its maximum displacement. The robot recovers back to the upright state. In all cases, the torques are similar: the ankle torques initially saturate at 50Nm if that torque is reached, and then smoothly decrease to zero; the hip torques initially grow and then decline to zero.

Fig. 4 shows the angle trajectories and the corresponding

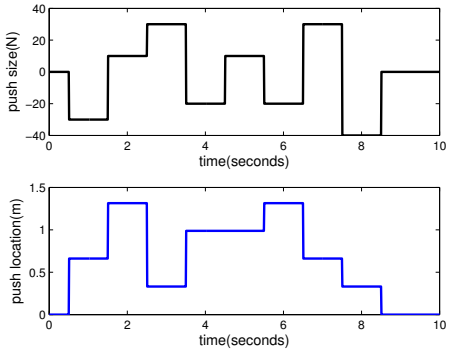

(a) Sequence of random push size and location.

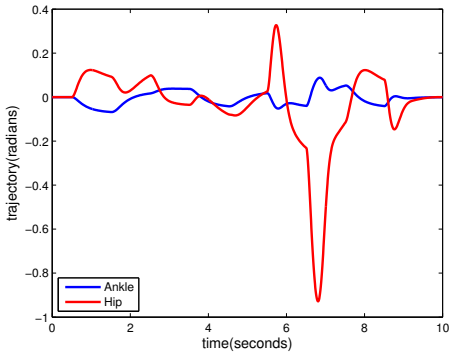

(b) The ankle and hip angle trajectories.

Fig. 5. Simulated performance of the parameterized controller for pushes with variable sizes and locations.

torques for a set of constant push sizes at the head. With the small push sizes, ankle and hip angles gradually scale with push magnitude, reaching the corresponding equilibrium states; ankle and hip torques smoothly decrease to zero, with ankle saturation. With the large push sizes, the robot initially responds to the posture with a large positive ankle angle and a negative hip angle, due to ankle torque saturation, and then smoothly approaches the corresponding equilibrium state; the ankle torque saturation persists longer and the hip torques increase from a small or even negative value to a large positive displacement and then decrease to zero.

The robustness of the proposed controllers are tested with a set of random pushes, using both instantaneous and constant perturbations. Fig. 5(a) shows the variable push sizes and locations, and the corresponding joint trajectories are presented in Fig. 5(b). After the end of the push at 8.5s, the robot recovers.

III. Balance Controller in the Lateral Plane

In the lateral plane (side to side motion), we use a six-link model, with torque actuators located at the ankles, hips, and waist and force actuators at the knees, as shown in Fig. 6. We employ a pair of telescoping knees and a waist to match human lateral balance behaviors. The telescoping knees have springs and dampers and are used to shorten or elongate the legs a little bit. The system parameters in the lateral plane are shown in Table I, where the CoM is the location of the

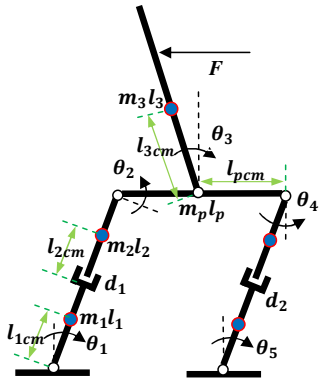

Fig. 6. Lateral model with 5 revolute joints and 2 prismatic knees.

center of mass relative to the lower joint and the MoI is the link moment of inertia about the CoM. The ankle, hip, and waist joint angles are bounded by $-0.45 < \theta_1 < 0.45$ radians, $-0.95 < \theta_2 < 0.95$ radians and $-0.95 < \theta_3 < 0.95$ radians. The ankle, hip and waist torques are limited within ± 167Nm, ± 107Nm and ± 245Nm, respectively, and the knee spring and damping constants are $K_s = 10^4$ and $\delta = 5 \times 10^3$. The properties of right leg joints are symmetric to the left ones.

A. Balance Controller

We define the state as prismatic knee lengths and velocities and revolute joint angles and angular velocities. The robot lateral dynamics are:

$$\mathbf{x}(k+1) = \boldsymbol{f}(\mathbf{x}(k), \tau(k), f(k), F(k), r(k)), \tag{4}$$

where $\mathbf{x} = (\theta_1, d_1, \ldots, \dot{d}_2, \dot{\theta}_5)^{\mathrm{T}}$ is the state vector, $\tau = (\tau_1, \tau_2, \tau_3, \tau_4, \tau_5)^{\mathrm{T}}$ are the joint torques, $f = (f_1, f_2)^{\mathrm{T}}$ are the knee forces, and F and r are the push size and location.

The feedback controller acts on state errors:

$$\begin{aligned} \tau_1 &= -k_1 \Delta\theta_1 - k_2 \Delta d_1 - \cdots, \\ f_1 &= -k_{15} \Delta\theta_1 - k_{16} \Delta d_1 - \cdots + f_{1\_d}, \\ &\vdots \\ \tau_5 &= -k_{85} \Delta\theta_1 - k_{86} \Delta d_1 - \cdots, \end{aligned} \tag{5}$$

where $f_{i\_d} = f_0 - K_s d_{i\_d}$ and d_{i_d} are the desired knee forces and knee lengthes for a determined equilibrium posture, f_0 is the knee force when the robot stands straight up,

$$\begin{aligned} \Delta\theta_i &= \theta_i - \theta_{i\_d}, \qquad & \Delta d_i &= d_i - d_{i\_d}, \\ \Delta\dot{\theta}_i &= \dot{\theta}_i - \dot{\theta}_{i\_d}, \qquad & \Delta\dot{d}_i &= \dot{d}_i - \dot{d}_{i\_d}, \end{aligned}$$

represent the error between actual state and the desired state of each joints: $\Delta\theta$ for revolute joints and Δd for prismatic joints.

The lateral dynamics consists of multiple model transitions between single and double support. We use an impact model with impulse effects, which assumes the contact is between two rigid bodies [10].

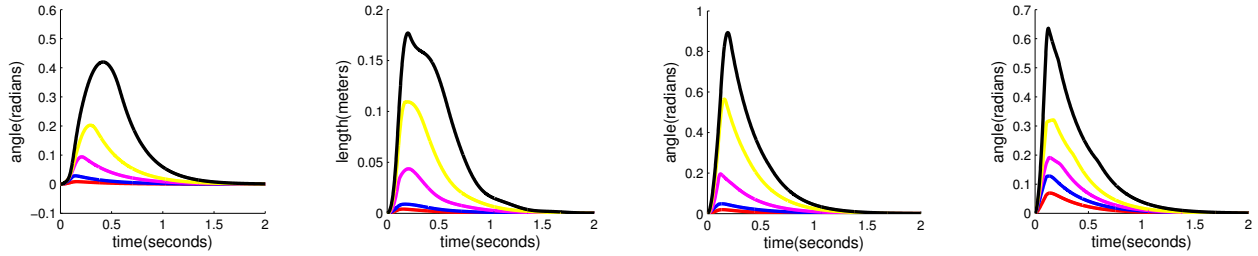

(a) Left ankle angle (b) Left knee length (c) Left hip angle (d) Torso angle

Fig. 7. Simulated joint trajectories of the lateral model for a range of impulsive perturbation sizes at the head (15, 30, 45, 60, 75 Newton-seconds).

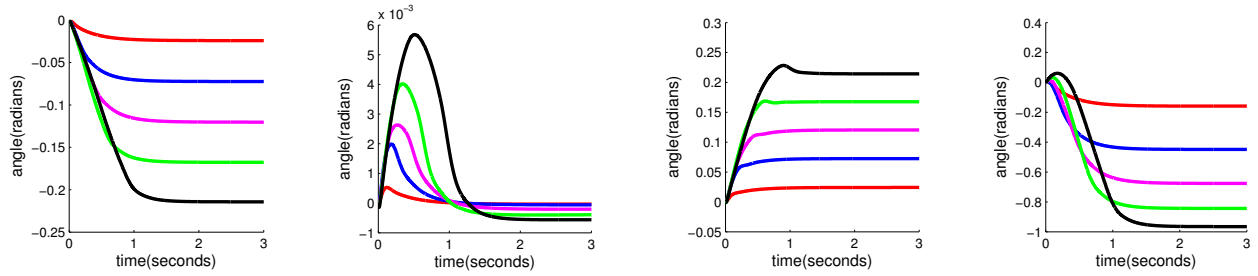

(a) Left ankle angle (b) Left knee length (c) Left hip angle (d) Torso angle

Fig. 8. Simulated joint trajectories of lateral model for a range of constant perturbation sizes at the head (15, 30, 45, 60, 75, 90 Newtons).

B. Optimization and Results

The one step optimization cost function in the lateral plane is:

$$\boldsymbol{L}(\mathbf{x},\mathbf{u}) = \mathrm{T}\left(\Delta\mathbf{x}^{\mathrm{T}}\mathbf{Q}\Delta\mathbf{x} + \tau^{\mathrm{T}}\mathbf{R}_1\tau + \Delta\boldsymbol{f}^{\mathrm{T}}\mathbf{R}_2\Delta\boldsymbol{f}\right), \qquad (6)$$

where T is the time step of the simulation (1ms), $\Delta\boldsymbol{f} = \boldsymbol{f} - \boldsymbol{f}_d$ is the error vector of the knee force, $\mathbf{Q} = \mathbf{I}_{14\times14}$, $\mathbf{R}_1 = 0.02\cdot\mathbf{I}_{5\times5}$, and $\mathbf{R}_2 = 0.02\cdot\mathbf{I}_{2\times2}$ are the corresponding weight matrices, where 0.02 weights the torque and force penalty relative to the state error.

We apply the previous optimization approach for both impulsive and constant pushes. In response to constant forces, the robot starts from vertical and moves to an equilibrium state, at which the torques of each joint are zero. For optimization, with the given push size and location, we choose as initial states five postures which are the equilibrium states for the pushes between zero and the given push. The controller has 98 parameters in the lateral plane.

Fig. 7 shows the left leg joint and the torso state trajectories generated by the optimized parametric controller in response to impulsive pushes at the head with a variety of sizes. Each trajectory roughly scales with the perturbation size and are all positive. The maximum displacements of each joint and the corresponding time are proportional to the perturbation magnitudes. Fig. 8 shows the behaviors of the left leg joints and the torso to a number of constant push sizes at the head. All trajectories are scaling with perturbation magnitudes, with the ankle and the hip moving directly to their equilibrium states. For the small pushes, the torso angles are entirely negative; for the large pushes, the ankle joint initially moves in the positive direction and then approaches its negative equilibrium state. In all cases, the left knee moves in the positive direction and then moves to its negative equilibrium state.

IV. Balance Controller in 3-Dimensions

For 3 dimensional balance, we use a six-link model with revolute joints, with 6 DOFs for each leg and one DOF at the waist. The joints are shown in Fig. 9. We apply the same model parameters, joint limits, and torque bounds as in the sagittal and lateral plane, adding two ankle yaw joints bounded by $-0.7 < \theta_3 < 0.7$ radians and replacing the telescoping knees with a pair of revolute knee joints ($0 < \theta_4 < 2$ radians, the knees can not bend forward). The torque ranges of the ankle yaw joints and knees are $\pm$74Nm and $\pm$293Nm, respectively. The properties of the two legs are symmetric. A 3-D impact model is employed between rigid bodies for model transitions [10].

A. Balance Controller

We consider the state as angles and angular velocities of each joint. The robot 3-D dynamics are:

$$\mathbf{x}(k+1) = \boldsymbol{f}(\mathbf{x}(k),\tau(k),F(k),r(k),\alpha(k)), \qquad (7)$$

where $\mathbf{x} = (\theta_1,\theta_2,\ldots,\dot{\theta}_{13})^{\mathrm{T}}$ is the state vector, $\tau = (\tau_1,\tau_2,\ldots,\tau_{13})^{\mathrm{T}}$ represent the joint torques, and F, r and α indicate the push size, location and direction, with $\alpha = 0$ representing a forward push in the sagittal plane and clockwise being positive.

The 3-D balance controller is linear in the error state:

$$\begin{aligned}
\tau_1 &= -k_1\Delta\theta_1 - k_2\Delta\theta_2 - \cdots,\\
\tau_2 &= -k_{27}\Delta\theta_1 - k_{28}\Delta\theta_2 - \cdots,\\
&\vdots\\
\tau_{13} &= -k_{313}\Delta\theta_1 - k_{314}\Delta\theta_2 - \cdots.
\end{aligned} \qquad (8)$$

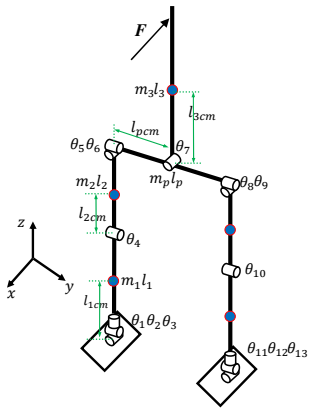

Fig. 9. The 3 dimensional model with 13 revolute joints.

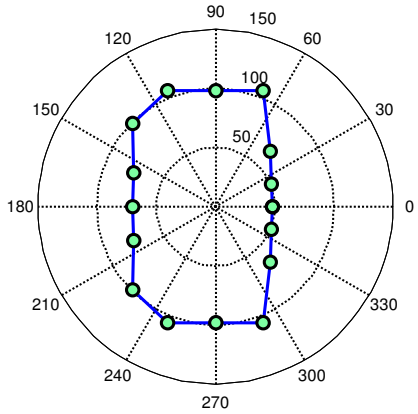

Fig. 10. The maximum balancing push area for a push at the head.

where $\Delta\theta_i = \theta_i - \theta_{i\_d}$ and $\Delta\dot{\theta}_i = \dot{\theta}_i - \dot{\theta}_{i\_d}$ represent the error between actual state and desired state of each joints. The outputs of the controller are limited to the given torque ranges.

We use a one step optimization cost function

$$\boldsymbol{L}(\mathbf{x},\mathbf{u}) = \mathrm{T}\Delta\mathbf{x}^{\mathrm{T}}\mathbf{Q}\Delta\mathbf{x} + \mathrm{T}\tau^{\mathrm{T}}\mathbf{R}\tau, \tag{9}$$

where T is the time step of the simulation (1ms), $\mathbf{Q} = \mathbf{I}_{26\times 26}$ and $\mathbf{R} = 0.02 \cdot \mathbf{I}_{13\times 13}$ are the weight matrices, where 0.02 weights the torque penalty relative to the state error. The sum of the one step cost function over each step constitutes the optimization criterion.

B. Results

We use the same approach to optimize the feedback gains for 3-D balance in response to a variety of push sizes, locations and directions. The controller has 338 parameters in 3-dimensions. For the proposed controller, Fig. 10 is the fall boundary for constant pushes located at the head. The circled points are the maximum constant push size for every $\pi/8$ radian. With knees, the 3D model controller is capable of handling larger forward and backward pushes than the planar sagittal controller.

V. Conclusions and Future Work

In this paper, feedback controllers in the sagittal, lateral plane and for the 3-D case are designed for standing balance in response to both impulsive and constant pushes. SNOPT is used to optimize parametric controllers for different push sizes, locations and directions. During a simulated perturbation experiment, the appropriate controller is continuously selected using a lookup table based on the current push or the last detected push for impulsive disturbances.

We also explore gain change with perturbation size. Using the optimized controller for constant pushes in the sagittal plane as an example, it appears that feedback gains gradually scale with push magnitude for small pushes and change significantly for large pushes. With increasing push size, the controller tends to increase the ankle gains while making some hip gains more negative. From the optimized feedback gains, we also find that the ankle joint plays an important role for small perturbations while the hip joint grows more active as the push size increases.

Future research will implement these controllers on an actual robot. We will explore the sensitivity of the approach to robot model parameters and optimization criterion parameters, which are currently selected by hand. We will develop a push size and location estimation to guide response selection.

VI. Acknowledgment

This material is based upon work supported in part by the US National Science Foundation under grants ECCS-0325383 and ECCS-0824077, and in part by the Program for New Century Excellent Talents in University (NCET-06-0398) and National Nature Science Foundation of China (NSFC Key project 60935001).

References

[1] S. Hyon, J. G. Hale and G. Cheng, "Full-body compliant human-humanoid interaction: balancing in the presence of unknown external forces", *IEEE Trans. Rob.*, vol. 23, no. 5, pp. 884-898, 2007.

[2] B. Stephens, "Integral control of humanoid balance", *Proc. IEEE Int. Conf. Intell. Rob. Syst.*, 2007, pp. 4020-4027.

[3] C. G. Atkeson and B. Stephens, "Multiple balance strategies from one optimization criterion", in *Proc. IEEE Int. Conf. human. robot.*, 2007.

[4] C. Liu and C. G. Atkeson, "Standing balance control using a trajectory library," *Proc. IEEE Int. Conf. Intell. Rob. Syst.*, 2009.

[5] A. D. Kuo, "An optimal control model for analyzing human postural balance", *IEEE Trans. Biomed. Eng.*, vol. 42, no. 1, pp. 87-101, 1995

[6] S. Park, F. B. Horak and A. D. Kuo, "Postural feedback responses scale with biomechanical constraints in human standing", *Experimental Brain Research*, vol. 154, no. 4, pp. 417-427, 2004.

[7] A. Alexandrov, A. Frolov, F. Horak, P. Carlson-Kuhta and S. Park, "Feedback equilibrium control during human standing", *Biol Cybern*, vol, 93, pp. 309-322, 2005.

[8] P. E. Gill, W. Murray and M.A. Saunders, "SNOPT: An SQP algorithm for large-scale constrained optimization", SIAM *J. Optim.*, pp. 979-1006.

[9] F. Orderud, "Comparison of Kalman filter estimation approaches for state space models with nonlinear measurements", in *Proc. Scandinavian Conf. Simulation Modeling*, 2005.

[10] M. Moore and J. Wilhelms, "Collision detection and response for computer animation", *Computer Graphics*, Vol. 22, No. 4, pp. 289-298, 1988.